Analysis of heat flow and "channelling" in a scraped-surface heat exchanger

A. D. Fitt · M. E. M. Lee · C. P. Please

Abstract Scraped-surface heat exchangers (SSHEs) are widely used in industries that manufacture and thermally process fluids; in particular, the food industry makes great use of such devices. Current understanding of the heat flow and fluid dynamics in SSHEs is predominantly based on empirical evidence. In this study a theoretical approach (based on asymptotic analysis) is presented for analysing both the flow and heat transfer in an idealised SSHE (a cylindrical annulus) for Newtonian fluids. The theory allows the effects of scraping-blade configuration, pumping rates, annular shear velocity and material properties all to be accounted for. The analysis relies on asymptotic simplifications that result from the large Péclet numbers and small geometrical aspect ratios that are commonly encountered in industrial SSHEs. The resulting models greatly reduce the computational effort required to simulate the steady-state behaviour of SSHEs and give results that compare favourably with full numerical simulations. The analysis also leads to what appears to be the first theoretical study on the undesirable phenomenon of "channelling", where fluid passes through the device in an essentially unheated or uncooled state. A parametric study is also undertaken to investigate the general circumstances under which channelling may occur.

Keywords Advection-driven thermal flow · Averaging · Lid-driven cavity · Lubrication theory · Scraped-surface heat exchanger

1 Industrial background

One of the food industry's constant goals is to reduce manufacturing costs whilst retaining control over food quality. The process optimisation of heat transfer is therefore a particular priority for the many food products that are made by heating or cooling a raw material or mixture of materials. A number of distinct

A. D. Fitt (✉) · C. P. Please
School of Mathematics, University of Southampton, Southampton SO17 1BJ, UK
e-mail: a.d.fitt@maths.soton.ac.uk

C. P. Please
e-mail: c.p.please@maths.soton.ac.uk

M. E. M. Lee
BP Institute for Multiphase Flow, University of Cambridge, Madingley Road, Cambridge CB3 0EZ, UK
e-mail: michael@bpi.cam.ac.uk

Fig. 1 Diagram of a typical Chemtech International Ltd. SSHE

Fig. 2 Cross-sectional diagram of a typical scraped-surface heat exchanger

types of heat exchangers are routinely used in the food sector. The fluid flow and heat transfer in classical plate and tubular heat exchangers is normally relatively straightforward and easy to understand and optimise. Matters are a great deal more complicated in scraped-surface heat exchangers (SSHEs) where both operational and modelling difficulties are often present. SSHEs are often used to process products that require more sophisticated heat-transfer mechanisms; an illustration of a Chemtech International Ltd. SSHE is shown in Fig. 1.

In devices such as that shown in Fig. 1, food is pumped axially through a long cylindrical annulus. The outer cylinder, sometimes called the stator, is heated or cooled and the inner "rotor" cylinder (which may be assumed to be thermally insulated) rotates at a prescribed velocity. Blades are attached to the rotor and continuously scrape foodstuffs from the stator, the heat-exchange surface. A typical SSHE cross-sectional configuration is shown in Fig. 2.

The materials that are processed in an SSHE encompass a broad spectrum of rheological behaviour. Some possess a yield stress and exhibit viscoelastic or pseudoplastic properties and many have a highly temperature-dependent viscosity. Some processed foods also involve multiphase flow and/or particle suspensions. Crystallisation, freezing and other phase changes may also take place. Generally, however, the main aim in SSHE operation is to ensure that the heat transfer from the stator to the food is both (a) maximised and (b) distributed as evenly as possible within the food. In order to achieve these twin goals, process engineers may alter many aspects of a particular machine. Blade configuration, annular gap width, axial length, rotation speed and pump pressure may all be changed not only for optimisation purposes, but also to avoid the occurrence of flow regimes that are regarded as undesirable. One such flow regime, which is normally to be avoided at all costs, involves "channelling". Under certain conditions large regions of the material being processed may pass through the heat exchanger in an essentially thermally unaltered fashion. The existence of such flow "channels" can render the final product completely useless.

How can channelling be avoided? Currently, the theoretical understanding of SSHEs is limited. Food manufacturers therefore usually rely on empirical knowledge, and may expend significant resources adapting operating parameters to new materials or products. The aim of this study is to try to produce a simplified model of flow and heat transfer in an SSHE and thereby allow the phenomenon of channelling to be approached from a theoretical point of view.

2 Preamble

A number of authors have previously modelled heat and fluid flow in SSHEs. All have assumed that the flow is laminar, and we will also make this assumption. Numerical approaches include a 3D simulation of the flow of a Newtonian liquid in an SSHE [1] and 2D cross-sectional studies [2, 3] of pseudoplastic materials with temperature-dependent viscosities; each of these studies involved substantial computational effort. Isothermal fluid flow analyses were undertaken in [4, 5] which both employed asymptotic analysis based on the small axial and transverse reduced Reynolds numbers. In [4], the behaviour of freely pivoted scraper blades in a Newtonian viscosity dominated liquid was considered and predictions were made of the conditions under which the blades could act successfully as scrapers. Isothermal pseudoplastic flow in an SSHE was studied in [5] where a throughput optimisation problem was also considered. Though the experimental studies [6, 7] of pseudoplastic isothermal fluid flow in an SSHE provided additional evidence supporting the asymptotic approach of [5], the relevance of purely isothermal studies of a process, whose ultimate object is heat exchange, is naturally limited. The aim of our work here is therefore to investigate the dependency of output temperature distribution on the design and process parameters.

Since we will consider fluid flows that are predominantly unaltered by thermal gradients, an asymptotic description similar to that used in [5] will be employed. Here, however, analysis of the heat transfer in the flow will be considered to be of paramount importance. In Sect. 3, a 3D "lubrication theory" model is presented, along with detailed discussion of the boundary conditions in the blade regions. We describe the structure of the heat-flow problem and compare model simulations with full numerical CFD results. In Sect. 4, this 3D model is simplified further and a 2D averaged equation and its solutions are investigated. This allows us to examine the dependence of SSHE output on operating parameters and to draw some theoretical conclusions regarding the phenomenon of "channelling".

3 3D "lubrication" model

We now present the scaling arguments for a "lubrication theory" model. This model will also form the basis of the further simplified model studied in Sect. 4. The approximation is valid everywhere, except near the scraper blades, and is derived by assuming that the reduced Reynolds number and the channel aspect ratios are both small. Near the blades, we propose a simple boundary condition (based on particle tracking and asymptotically negligible residence times) that allows us to avoid the complications of full numerical 3D computations; a comparison with a full CFD simulation is given to outline the potential strengths and weaknesses of the model used.

We begin by stating the full problem. Since processing typically occurs over a period of hours ($\mathcal{O}(10^4\,\mathrm{s})$) or sometimes days, and particle residence times are of $\mathcal{O}(10\,\mathrm{s})$, we assume that a steady state prevails. The governing Navier–Stokes and energy equations are (the summation convention has been used)

$$\frac{\partial u_k}{\partial x_k} = 0, \tag{1}$$

$$\rho u_k \frac{\partial u_i}{\partial x_k} = -\frac{\partial p}{\partial x_i} + 2\frac{\partial}{\partial x_k}(\mu e_{ik}), \tag{2}$$

$$\rho c_p u_k \frac{\partial T}{\partial x_k} = \frac{\partial}{\partial x_k}\left(k\frac{\partial T}{\partial x_k}\right) + 2\mu e_{kl}\frac{\partial u_k}{\partial x_l}. \tag{3}$$

Table 1 Typical values (SI units) for SSHE parameters (L based on 2 or 3 blade configurations)

	k	c_p	ρ	U	W	$\frac{\mu}{\rho}$	G	H	L	a
Chemtech	0.4	4	800	2.0	0.2	0.1	2.0	0.015	0.15	0.075
Tetra Pak	0.5	3.5	1000	0.2	1.5	0.4	2.0	0.016	0.2	0.061

Here u_i are the components of the fluid velocity $\boldsymbol{u}$, $e_{ij} = \frac{1}{2}\left(\partial u_i/\partial x_j + \partial u_j/\partial x_i\right)$ is the infinitesimal rate-of-strain tensor, p is the fluid pressure and T the temperature. The material properties are denoted by ρ (density), c_p (specific heat) and k (thermal conductivity), all of which are assumed to be constant. The boundary conditions are

$$\boldsymbol{u} = 0 \text{ and } T = T_s \quad \text{at } r = a + H, \tag{4}$$

$$\boldsymbol{u} = U\boldsymbol{e}_\theta \text{ and } \frac{\partial T}{\partial r} = 0 \quad \text{at } r = a, \tag{5}$$

$$\boldsymbol{u} = U\boldsymbol{e}_\theta \text{ and } \frac{\partial T}{\partial n} = 0 \text{ on the surface of each scraper}, \tag{6}$$

where T_s is the prescribed stator temperature, n is normal to the blade surface and the cylindrical polar unit vectors $(\boldsymbol{e}_r, \boldsymbol{e}_\theta)$ lie in the transverse (cross-sectional) plane as illustrated in Fig. 2. To complete the problem specification it is necessary to prescribe suitable conditions at the inlet and outlet. In general, the solution to this three-dimensional problem requires demanding numerical computation (see, for example [1,8]). However, we will try below to analyse "channelling" by employing asymptotic analysis.

3.1 Scalings and asymptotic analysis

We begin by presenting, in Table 1, some typical operating parameters from two of our industrial collaborators. In the table W and G denote axial velocity and length-scale, respectively. Note that, though the values (in particular those related to material properties) may vary substantially depending on what sort of food is being processed, the aspect ratios ϵ and L/G are almost invariably small.

   Since the annular gap-width/rotor-radius ratio H/a is small, we assume that flow takes place in a periodic parallel channel as shown in Fig. 3. We also use a frame of reference that rotates with the blades and rotor so that the stator now moves at speed U. The problem may be decomposed into periodic (and adjacent) blade and cavity regions which are assumed to have lengths l and L, respectively. We address problems where $(l/L) \ll 1$ so that the blade regions are relatively short. We therefore focus our attention on the fluid dynamics in the periodic cavity. The case where the blade penetration height h_1 is equal to the channel height H, so that the blades completely block the channel, resembles the classical fluid-dynamics problem of a lid-driven cavity; this was studied in the context of an SSHE in [5, 8].

   To non-dimensionalise the problem, we use the scalings

$$x = L\bar{x}, \quad y = \epsilon L\bar{y}, \quad z = \alpha L\frac{\bar{z}}{\epsilon},$$

$$\boldsymbol{u} = U(\bar{u}, \epsilon\bar{v}, \epsilon\bar{w})^T, \quad T = T_s + (T_{in} - T_s)\bar{T}, \quad p = p_a + \frac{\mu U}{L\epsilon^2}\bar{p}, \tag{7}$$

where $\epsilon = H/L$ denotes the transverse aspect ratio, $\alpha = \epsilon(G/L) = \mathcal{O}(1)$, T_{in} is the inlet temperature at $z = 0$, and an over-bar refers to a non-dimensional, order unity variable. These scalings are equivalent to a "lubrication theory" approach, where both the reduced Reynolds number $\epsilon^2\text{Re} = \epsilon^2\left(\rho UL/\mu\right) \ll 1$ and the aspect ratio $\epsilon \ll 1$. In this limiting case (1)–(2) become, to leading order,

Fig. 3 A cross-sectional diagram of periodic cavities and blade-array regions
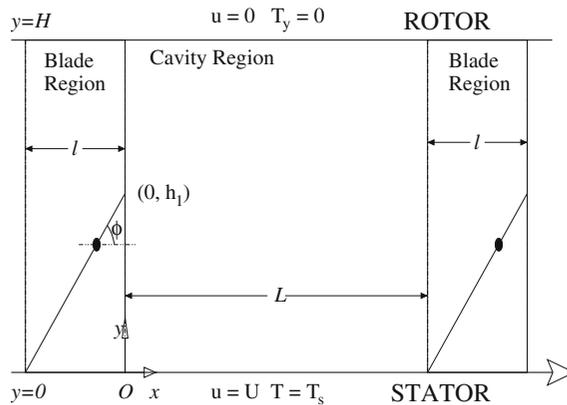
$$\frac{\partial \bar{u}}{\partial \bar{x}} + \frac{\partial \bar{v}}{\partial \bar{y}} = 0, \tag{8}$$

$$\frac{\partial^2 \bar{u}}{\partial \bar{y}^2} - \frac{\partial \bar{p}}{\partial \bar{x}} = 0, \quad -\frac{\partial \bar{p}}{\partial \bar{y}} = 0, \quad \alpha \frac{\partial^2 \bar{w}}{\partial \bar{y}^2} - \frac{\partial \bar{p}}{\partial \bar{z}} = 0. \tag{9}$$

Note that the centripetal acceleration, Coriolis and gravity terms have all been ignored in deriving (8) and (9). It transpires that the largest centripetal term (which appears in the x-momentum equation) is of order $L^3 \epsilon^2 / \nu a$, the Coriolis term is of order $2U\epsilon^3 L^2 / \nu a$ and the largest gravity term (which appears in the z-momentum equation) is of order $g\epsilon L^2 / \nu U$. Using the values from Table 1, all of these terms are seen to be much less than unity and may therefore be ignored.

The flow is viscosity-dominated, fully developed and laminar; to leading order, axial and transverse components of the fluid motion can be treated separately and mass in the transverse plane is globally conserved. The solution to (9), with $\bar{u} = 1$, $\bar{w} = 0$ at $\bar{y} = 0$ and $\bar{u} = \bar{w} = 0$ at $\bar{y} = 1$, is

$$\bar{u} = (6Q\bar{y} + (1 - 3\bar{y}))(1 - \bar{y}), \quad \bar{v} = 0, \quad \bar{w} = \lambda \bar{y}(1 - \bar{y}), \quad \bar{p} = -2\lambda \alpha \bar{z} + 2(3 - 6Q)\bar{x}. \tag{10}$$

The quantity $Q = Q_x / \rho UH$ denotes the dimensionless transverse flux (produced by flow over the blades between adjoining chambers), and involves the transverse mass flux Q_x per unit z-direction length (dimensions kg/m/s) defined by

$$Q_x = \int_0^H \rho u \, dy.$$

The axial mass flux Q_z (dimensions kg/s) is defined exactly by

$$Q_z = \int_{\theta=0}^{2\pi} \int_{r=a}^{r=a+H} \rho w r \, dr \, d\theta.$$

Since in our approximation $H \ll a$, it is consistent to assume that $NL = 2\pi a$ where N denotes the number of scrapers. Thus

$$Q_z \simeq NL \int_0^H \rho w \, dy$$

and, using (10), $\lambda = 6Q_z / (N\rho UH^2)$. The dimensionless quantity λ thus represents a ratio of the axial velocity induced by pumping to the circumferential velocity induced by rotation. Normally a process operator may control both the transverse and axial flux; the former is altered by changing the blade geometry or configuration and the latter by altering the pumping rate. In our analysis below we will assume that Q_x is simply prescribed. If, however, the reduced Reynolds number $\epsilon^2 \rho UL / \mu \ll 1$ in the blade region, then,

using the calculations of [4], the inter-cavity transverse flux can be related to blade angle ϕ and height h_1 (see Fig. 3).

The remaining governing field equation is the energy balance (3), and by applying the scalings (7) we find that, to leading order,

$$\frac{1}{\gamma}\left(\bar{u}(\bar{y};Q)\frac{\partial\bar{T}}{\partial\bar{x}} + \delta\hat{w}(\bar{y})\frac{\partial\bar{T}}{\partial\bar{z}}\right) = \frac{\partial^2\bar{T}}{\partial\bar{y}^2} + \mathrm{Br}\left(\frac{\partial\bar{u}}{\partial\bar{y}}\right)^2 + O(\mathrm{Br}\epsilon^2,\epsilon^2), \tag{11}$$

where

$$\gamma^{-1} = \epsilon^2\mathrm{Pe}, \quad \delta = \frac{\epsilon^2\lambda}{\alpha} = \frac{3Q_z}{\pi N G \rho U H} \quad \text{and} \quad \hat{w} = \bar{y}(1-\bar{y}). \tag{12}$$

The reciprocal of γ is a reduced Péclet number and δ may be thought of as a ratio of axial to transverse velocity. We have introduced $\hat{w}$ so, that the process parameter δ is more clearly visible in (11). The Péclet number, the product of the Prandtl and Reynolds numbers, characterises the ratio of advection to heat diffusion and is defined as

$$\mathrm{Pe} = \frac{\mu c_p}{k}\frac{\rho U L}{\mu} = \mathrm{Pr}\,\mathrm{Re}.$$

Based on the values in Table 1, we see that $\epsilon = \mathcal{O}(10^{-1})$, $\epsilon^2\mathrm{Re} = \mathcal{O}(10^{-2})$ or less, $\mathrm{Pe} = \mathcal{O}(10^3)$ and $\gamma = \mathcal{O}(10^{-2})$. The Brinkman number

$$\mathrm{Br} = \frac{\mu U^2}{k(T_{\mathrm{in}} - T_{\mathrm{s}})},$$

characterises the ratio of viscous dissipation to heat diffusion. For the Tetra Pak machine $\mathrm{Br} \sim \mathcal{O}(1)$ when the temperature difference $T_{\mathrm{in}} - T_{\mathrm{s}}$ is about $10°\mathrm{C}$ (for the Chemtech machine Br is approximately 10 when the temperature difference is $80°\mathrm{C}$, but $\epsilon^2\mathrm{Br} \ll 1$). We conclude from these parameter estimates that the temperature equation (11) is advection-driven (u being dominant over w), but also includes viscous dissipation and radial diffusion (in the y-direction) between rotor and stator. For the model to be valid we require

$$\epsilon^2\mathrm{Re}, \quad \epsilon^2, \quad \gamma \text{ and } \epsilon^2\mathrm{Br} \ll 1.$$

Note that the constraints on the reduced Reynolds and inverse reduced Péclet numbers and aspect ratios are fundamental to the problem formulation, whereas if the reduced Brinkman number $\epsilon^2\mathrm{Br}$ were to be of order unity or larger, additional viscous dissipation terms could be included.

By application of the scalings (7), the thermal boundary conditions in (4)–(6) become

$$\bar{T} = 1 \quad \text{at } \bar{z} = 0, \quad \frac{\partial\bar{T}}{\partial\bar{y}} = 0 \quad \text{at } \bar{y} = 1, \quad \bar{T} = 0 \quad \text{at } \bar{y} = 0. \tag{13}$$

To complete the problem defined so far by (11) and (13) we need to consider the flow near the blades in the blade regions at $\bar{x} = 0$ and $\bar{x} = 1$. This aspect of the problem is non-trivial and would normally require solving the full problem (1)–(3) in boundary layers of size $\mathcal{O}(\epsilon)$ at $\bar{x} = 0$ and $\bar{x} = 1$ where the fluid flow ceases to be two-dimensional. However, since we are considering advection-dominated thermal flow we shall see that it will be possible to reduce the problem here to a simple "mapping condition" described in Sect. 3.2.

An examination of the terms in (11) when $\gamma \ll 1$ and $\delta \ll 1$ reveals that the thermal boundary layers on the rotor and stator, respectively, are of different types, with correspondingly different "entry region" lengths. For the rotor, where the flow is primarily of shear type, the entry length has size $\bar{z} = O(\delta)$ and the thermal boundary layer thickness is $O(\gamma^{1/3})$. For the stator, where the x-component of the velocity is nearly constant and the z-component is of shear type, the entry length has size $\bar{z} = O(\delta\gamma^{1/2})$ and the thermal boundary layer thickness is $O(\gamma^{1/2})$.
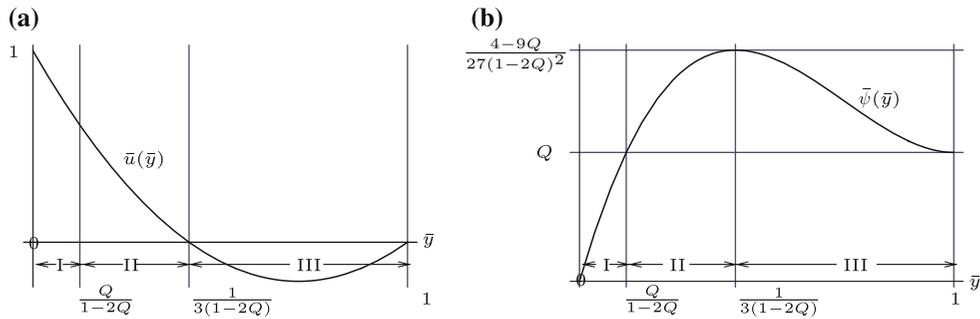
Fig. 4 An illustration of the flow speed $\bar{u}$ in the case $0 < Q < 1/3$ from (10) and stream function from (14) with regions I, II and III marked accordingly. (**a**) Velocity profile and (**b**) stream function

3.2 Fluid and heat flow near the blades

We begin by describing the fluid flow (10) arising from the "lubrication model" (8)–(9) in more detail. To leading order, mass is conserved in the transverse plane and it will be convenient to introduce a stream function $\bar{\psi}$, such that $\bar{u} = \partial\bar{\psi}/\partial\bar{y}$, $\bar{v} = -\partial\bar{\psi}/\partial\bar{x}$ and

$$\bar{\psi} = 6Q\left(\frac{\bar{y}^2}{2} - \frac{\bar{y}^3}{3}\right) + \bar{y}^3 - 2\bar{y}^2 + \bar{y}. \tag{14}$$

The topology of the flow inside the heat-exchanger cavity now depends on the size of the quantity Q. A number of cases may be identified:

3.2.1 Flow for $0 < Q < 1/3$

An examination of $\bar{\psi}$ and $\bar{u}$ shows that, in this case, we have forward flow for $0 < \bar{y} < 1/(3(1-2Q))$. Further, $\bar{u}$ decreases as $\bar{y}$ increases, reaching 0 at $\bar{y} = 1/(3(1-2Q))$. Reverse flow with $\bar{u} < 0$ takes place in the region $1/(3(1-2Q)) < \bar{y} < 1$; the reverse flow speed has a maximum at $\bar{y} = (3Q-2)/(3(2Q-1))$ where $\bar{u} = (9Q^2-6Q+1)/(3(2Q-1))$; thereafter the reverse flow speed decreases until at $\bar{y} = 1, \bar{u} = 0$ once again. Since, in practice, values of Q tend to be small, this is the case upon which we will expend most of our effort; plots of $\bar{u}$ and $\bar{\psi}$ for $0 < Q < 1/3$ are shown in Fig. 4. We identify three regions, labelled I, II and III in Fig. 4. Region I (where $\bar{u} \geq 0$, $0 \leq \bar{y} \leq Q/(1-2Q)$ and $0 \leq \bar{\psi} \leq Q$) is composed solely of fluid that has leaked over the scrapers from an adjacent cavity. In region II $\bar{u} \geq 0$, $Q/(1-2Q) \leq \bar{y} \leq 1/(3(1-2Q))$, $\bar{\psi}$ increases with increasing $\bar{y}$ and $Q \leq \bar{\psi} \leq (4-9Q)/(27(1-2Q)^2)$. In region III we have $\bar{u} \leq 0$, $1/(3(1-2Q)) \leq \bar{y} \leq 1$, $\bar{\psi}$ decreases with increasing $\bar{y}$, and $Q \leq \bar{\psi} \leq (4-9Q)/(27(1-2Q)^2)$. Regions II and III are both composed of fluid that remains trapped, recirculating in a given inter-scraper cavity.

3.2.2 Flow for $Q = 0$

When $Q = 0$ matters are simplified as there is no leakage from adjacent chambers. The scraper blades block the flow completely and all of the fluid recirculates between the blades, remaining in its specific cavity. Region I disappears but regions II and III remain as described above.

3.2.3 Flow for $Q \geq 1/3$

When $Q \geq 1/3$ the leakage between adjacent cavities dominates the flow, regions II and III disappear and only region I, where $0 \leq \bar{y} \leq 1$ and $\bar{\psi}$ increases monotonically with increasing $\bar{y}$ from 0 to Q survives: no fluid particle now remains trapped in a single inter-blade cavity and there is no reverse flow so that $\bar{u} \geq 0$
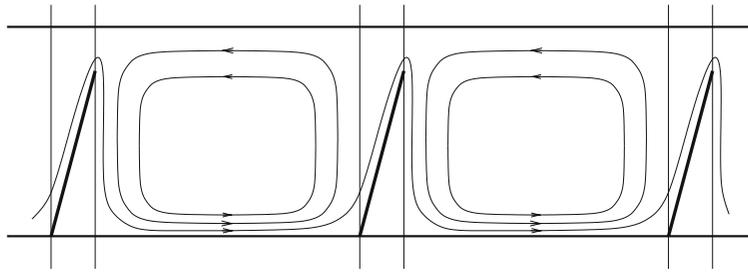
Fig. 5 An illustration of the transverse streamlines for a periodic array of scraping blade and cavities

for all $\bar{y} \in [0, 1]$. For $Q = 1/2$ the flow is of pure Couette type with a linear velocity profile; for $Q > 2/3$ an internal maximum flow speed exists at $\bar{y} = (2 - 3Q)/(3(1 - 2Q))$ where $\bar{u} = (9Q^2 - 6Q + 1)/(3(2Q - 1))$. Though this case could be further analysed with profit, we do not do so here, as it characterises a regime not normally found in SSHEs.

3.2.4 Cavity boundary conditions when $0 \leq Q < 1/3$

We now concentrate solely on the most practically realistic case when $Q < 1/3$. In the boundary layers of size $\mathcal{O}(\epsilon)$ at $\bar{x} = 0$ and $\bar{x} = 1$, we expect a streamline in region II to re-connect to a streamline in region III. The fluid in region I will move between cavities through the boundary layers; particles will leave a cavity at $\bar{x} = 1$ and re-enter the next cavity at $\bar{x} = 0$ with the value of the stream function preserved. Note that, viewed three-dimensionally, all particles will follow helical trajectories; those particles that begin in region I will circumnavigate the rotor periodically, whereas those that begin in regions II or III will remain between the same two adjacent blades. Figure 5 shows the planar projection of these helical motions. Our observations based on the stream function show good agreement with full numerical simulations in [1, 8].

Since the Péclet number is large, the temperature of a fluid particle will remain essentially constant as it moves through the boundary layers near the blade regions. Periodic-type boundary conditions may thus be prescribed at $\bar{x} = 0$ and $\bar{x} = 1$ using the stream function "re-connections" discussed above. We have

$$\bar{T}(0, \bar{y}_{\mathrm{II}}, \bar{z}) = \bar{T}(0, \bar{y}_{\mathrm{III}}, \bar{z}) \quad \left(\frac{Q}{1 - 2Q} < \bar{y} < 1 \right), \tag{15}$$

$$\bar{T}(1, \bar{y}_{\mathrm{III}}, \bar{z}) = \bar{T}(1, \bar{y}_{\mathrm{II}}, \bar{z}) \quad \left(\frac{Q}{1 - 2Q} < \bar{y} < 1 \right), \tag{16}$$

$$\bar{T}(0, \bar{y}_I, \bar{z}) = \bar{T}(1, \bar{y}_I, \bar{z}), \quad \left(0 < \bar{y}_I < \frac{Q}{1 - 2Q} \right), \tag{17}$$

where for a given value of $\bar{y} = \bar{y}_{\mathrm{II}}$ in region II say, $\bar{y}_{III}$ is determined by $\bar{\psi}(\bar{y}_{III}) = \bar{\psi}(\bar{y}_{II})$. The "reconnections" and region boundaries are shown schematically in Fig. 6.

The heat-transfer problem to be solved is therefore Eq. 11 (with $(\bar{x}, \bar{y}, \bar{z}) \in [[0, 1] \times [0, 1] \times [0, 1]]$) subject to conditions (13) and (15)–(17), with $\bar{\psi}$ defined by (14) and $\bar{u}$ and $\hat{w}$ defined by (10) and (12), respectively.

3.3 Numerical solution

The heat-transfer problem described above is relatively easy to solve numerically. We used a standard implicit finite-difference scheme to integrate down the exchanger, employing a cubic spline to impose the "connection" conditions (15) and (16) (for brevity we omit the full details). To validate our theoretical approach, we compared the numerical solution obtained to (11) (hereafter termed "modelling results")
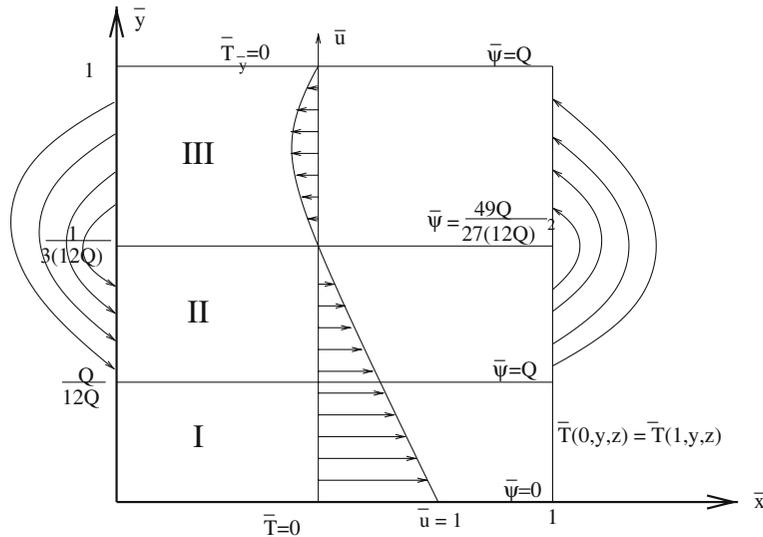
**Fig. 6** Schematic diagram of "reconnection" boundary conditions for $Q > 0$

with a full CFD numerical solution (hereafter termed "CFD"). To obtain CFD predictions, we used the results calculated in [8], where (1)–(3) were solved subject to the boundary conditions (6) and (13), in a 3D rectangular lid-driven cavity, using the commercial software package FASTFLO. The numerical results were carefully verified for both convergence and accuracy: for further details see [8] (and also [2, 3]). Cross-sectional contour plots of isotherms for both CFD and modelling results are shown in Fig. 7.

We observe in Fig. 7 that in both simulations the fluid is cooled in a boundary layer on the stator at $\bar{y} = 0$, and then transported onto stationary surfaces where the thermal boundary layer width is larger. The "reconnection" conditions imposed in our model, namely (15)–(17), assume that the fully two-dimensional flow regions adjacent to the blades are small in extent. Therefore, although detailed comparisons for the aspect ratio $\epsilon = 1/5$ (a typical value for industrial SSHEs) are not particularly good, it is evident that the temperature contours from the modelling results correctly predict both the qualitative and much of the quantitative behaviour between $\bar{x} \approx 1/5$ and $\bar{x} \approx 4/5$ (as predicted in Sect. 3). For transverse aspect ratios smaller than $\epsilon = 1/5$, the model will also provide good quantitative approximations. Similar comparisons may be made with many other numerical results: the conclusions are much the same.

4 Parametric investigations and channelling prediction

Now that we have derived a simplified model for an "idealised" SSHE in Sect. 3, we proceed with a parametric study in order to understand how the problem control parameters influence the heat-treatment process and, more specifically, to identify conditions under which channelling may occur. The numerical calculations of the heat flow given in Sect. 3.3 are reasonably time-consuming and so a further simplified model will be presented that allows us to study the parameter space $(\delta, \gamma, \mathrm{Br}, Q)$ with greater ease. Of particular interest to designers and process engineers is the thermally unaffected central region, as illustrated in Fig. 7. As operating parameters are altered, this unaffected region can be reduced or extended axially down the exchanger. If this region extends to the exit of the exchanger, this produces the unwanted effect of "channelling". The analysis below focuses on parameter regimes where this phenomenon occurs. It should be noted that the occurrence of channelling for a constant-viscosity fluid would be exacerbated if heat-thinning or shear-thinning effects were introduced, but we shall not quantify this here.

Fig. 7 Results for the
case $Q = 0$, $\gamma = 1/3200$,
Br= 0.512, $\delta = 1/8$ —
comparison of CFD
results (upper plots) with
$\epsilon = 1/5$ and "modelling"
results (lower plots). The
plots are shown for two
points ($\bar{z} = 0.4$ and
$\bar{z} = 0.6$). Isotherms have
intervals of 10^{-1} and are
scaled to the range [0,1]
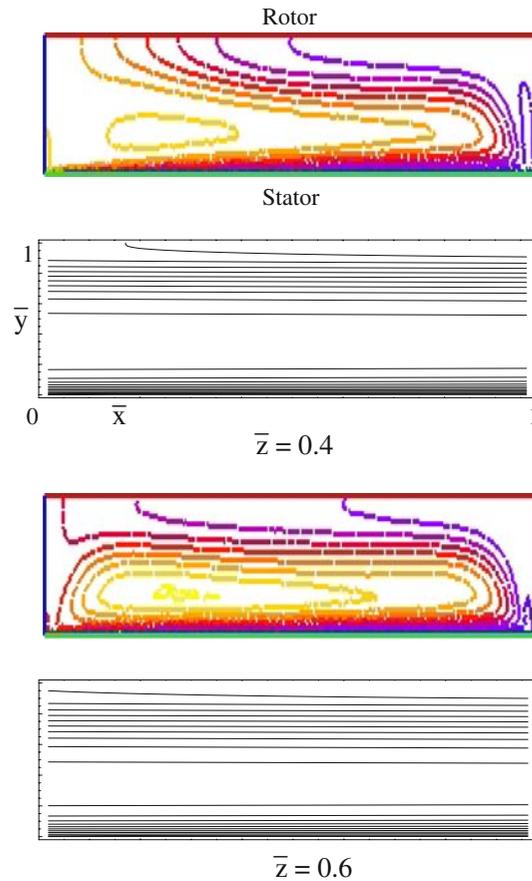
4.1 x-Averaged model

For simplicity we shall henceforth disregard the dimensionless notation over-bar. Based on our previous consideration of parameter sizes from Table 1, we consider the limits Br= $\mathcal{O}(1)$, $\gamma \to 0$ and $\delta \to 0$ in the distinguished limit $\delta = \mathcal{O}(\gamma)$. Physically, this represents the case where dissipation is important, the Péclet number is large and the flow around the exchanger is much faster than the flow down it. We seek an asymptotic solution of the form

$$T(x,y,z) = T_0 + \gamma T_1 + \mathcal{O}(\gamma^2). \tag{18}$$

Substitution of (18) in the governing equation (11) gives the $\mathcal{O}(1)$ balance

$$u(y;Q)\frac{\partial T_0}{\partial x} = 0. \tag{19}$$

This states that the leading-order temperature is independent of x, so that $T_0 = F(y,z)$, and the temperature will be constant along streamlines $T_0(\psi, z)$. To derive a governing equation for T_0 we consider the $\mathcal{O}(\delta, \gamma)$ terms and arrange as follows

$$\frac{\partial T_1}{\partial x} + \frac{\delta \hat{w}(y)}{\gamma u(y;Q)}\frac{\partial T_0}{\partial z} = \frac{1}{u(y;Q)}\frac{\partial^2 T_0}{\partial y^2} + \frac{\mathrm{Br}}{u(y;Q)}\left(\frac{\mathrm{d}u}{\mathrm{d}y}\right)^2. \tag{20}$$

An integration of (20) with respect to x will produce an averaged equation for T_0 once the boundary conditions (15)–(17) have been applied. The streamwise-mapping conditions (15) and (16) can be applied more easily when we change variables from y to ψ using (14), so Eq. 20 becomes

$$\frac{\partial T_1}{\partial x} + \frac{\delta \hat{w}}{\gamma u} \frac{\partial T_0}{\partial z} = u \frac{\partial^2 T_0}{\partial \psi^2} + \frac{u_y}{u} \frac{\partial T_0}{\partial \psi} + \frac{\mathrm{Br}}{u} \left(\frac{\mathrm{d}u}{\mathrm{d}y} \right)^2 . \tag{21}$$

Equation 21 involves both $T_1(x, y, z)$ and $T_0(y, z)$; to generate an equation that allows T_0 to be determined we employ a "Fredholm alternative" type argument in each flow region. First, consider region I and suppose that $y = y_I$. Integration of (21) from $x = 0$ to $x = 1$ gives (upon using (17) and observing that u, $\hat{w}$ and T_0 are all independent of x)

$$\frac{\delta \hat{w}_I}{\gamma u_I} \frac{\partial T_0}{\partial z} = u_I \frac{\partial^2 T_0}{\partial \psi^2} + \frac{u_{yI}}{u_I} \frac{\partial T_0}{\partial \psi} + \mathrm{Br} \frac{u_{yI}^2}{u_I} \quad (0 < \psi < Q), \tag{22}$$

thus giving an equation for T_0 in region I.

To determine an equation for T_0 in regions II and III, we integrate (21) from $x = 0$ to $x = 1$ first for $y = y_{II}$ in region II and then for $y = y_{III}$ in region III, yielding

$$T_1(1, y_{II}, z) - T_1(0, y_{II}, z) + \frac{\delta \hat{w}_{II}}{\gamma u_{II}} \frac{\partial T_0}{\partial z} = u_{II} \frac{\partial^2 T_0}{\partial \psi^2} + \frac{u_{yII}}{u_{II}} \frac{\partial T_0}{\partial \psi} + \mathrm{Br} \frac{u_{yII}^2}{u_{II}}$$

and a similar equation, but with subscripts II replaced by III. Subtracting and using (15) and (16) now gives

$$\frac{\delta}{\gamma} \left(\frac{\hat{w}_{II}}{u_{II}} - \frac{\hat{w}_{III}}{u_{III}} \right) \frac{\partial T_0}{\partial z} = (u_{II} - u_{III}) \frac{\partial^2 T_0}{\partial \psi^2} + \left(\frac{u_{yII}}{u_{II}} - \frac{u_{yIII}}{u_{III}} \right) \frac{\partial T_0}{\partial \psi}$$
$$+ \mathrm{Br} \left(\frac{u_{yII}^2}{u_{II}} - \frac{u_{yIII}^2}{u_{III}} \right) \quad \left(Q < \psi < \frac{4 - 9Q}{27(1 - 2Q)^2} \right). \tag{23}$$

We note that (22) and (23) are convection-diffusion type equations with timelike direction z that require the prescription of suitable boundary and initial conditions. At the inlet $z = 0$ and the stator $\psi = 0$ we have, respectively,

$$T_0(\psi, 0) = 1, \qquad T_0(0, z) = 0. \tag{24}$$

At the interface between regions II and III where $y = 1/(3(1 - 2Q))$ and $\psi = (4 - 9Q)/(27(1 - 2Q)^2)$, we impose continuity in both the temperature and the heat flux. Since $\partial T_0/\partial y = (\partial T_0/\partial \psi)(\partial \psi/\partial y)$ and $\partial \psi/\partial y = 0$ here, we must ensure that $\partial T_0/\partial \psi$ is non-singular. This is most easily imposed in practice by expanding (23) in a Taylor series for T_0 about $y = 1/(3(1 - 2Q))$. This shows that singular behaviour in $\partial T_0/\partial \psi$ may be avoided by imposing the Neumann condition

$$\frac{\delta}{\gamma} \left(\frac{\hat{w}_{II}}{u_{II}} - \frac{\hat{w}_{III}}{u_{III}} \right) \frac{\partial T_0}{\partial z} = \left(\frac{u_{yII}}{u_{II}} - \frac{u_{yIII}}{u_{III}} \right) \frac{\partial T_0}{\partial \psi} + \mathrm{Br} \left(\frac{u_{yII}^2}{u_{II}} - \frac{u_{yIII}^2}{u_{III}} \right) \quad \left(\psi = \frac{4 - 9Q}{27(1 - 2Q)^2} \right). \tag{25}$$

Finally, we require boundary conditions on the streamline $\psi = Q$ that separates the intra-cavity recirculating regions II and III and the inter-cavity through-flow region I. Again, we require that both the temperature and the heat flux are continuous. Continuity of temperature implies that

$$\lim_{\psi \to Q^+} T_0(Q, z) = \lim_{\psi \to Q^-} T_0(Q, z). \tag{26}$$

To ensure continuity of the heat flux, we recall that, although the heat flux at $\psi = Q^+$ involves the two boundaries $y = 1/(3(1 - 2Q))$ and $y = 1$, the boundary at $y = 1$ is insulated. The appropriate flux balance is therefore

$$\lim_{\psi \to Q^+} \frac{\partial T_0}{\partial \psi} = \lim_{\psi \to Q^-} \frac{\partial T_0}{\partial \psi}. \tag{27}$$

Fig. 8 Isotherms in the y–z plane derived using the averaged model of Sect. 4.1, with the recirculation (II and III) and leakage region (I) boundaries marked by two vertical lines; the parameters used were $\gamma = 10^{-2}, \delta = 10^{-1}$, $\gamma \mathrm{Br} = 10^{-3}$ and $Q = 0.1$. Contour intervals of 0.05 are shown and $0 < T_0 < 0.05$ defines the black region
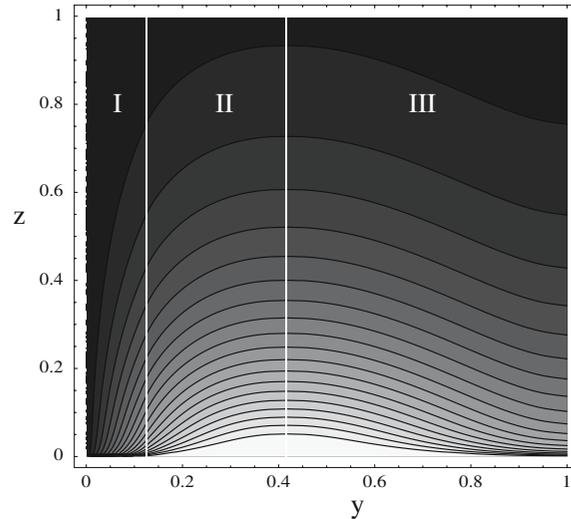
The complete problem for the average temperature, $T_0(\psi, z)$, is therefore defined by the Eqs. 22 and 23, along with boundary conditions (24)–(27).

Before discussing numerical solutions to the averaged problem, it is worth briefly discussing the case $Q = 0$, where there is no inter-cavity through-flow and region I does not exist. In this case the boundary at $\psi = 0$ corresponds to the two points $y = 0$ and $y = 1$ at which homogeneous Dirichlet and Neumann conditions are imposed, respectively. The condition $T = 0$ at $y = 0$ has the effect of cooling the flow and, consequently, a thermal boundary layer develops. The condition $T_y = 0$ imposed at $y = 1$ will only alter the size of this layer after it is transported through the blade region by the mapping conditions (15) and (16). Therefore, in the case $Q = 0$, we still impose the boundary conditions specified in (24).

4.2 Numerical results

Solutions to (22)–(27) were obtained using a standard implicit finite-difference method. The point $\psi = Q$ was always chosen to lie on a grid point and consequently a ghost point was required for the boundary at $\psi = (4 - 9Q)/(27(1 - 2Q)^2)$; for brevity we omit further details of the numerical scheme, which are of a standard nature. Figure 8 shows typical results from the averaged model, displayed as a plot of the thermal contours. (For ease of interpretation, the results have been "un-mapped" from ψ-space to y-space.) In the example shown, the parameters $\gamma = 10^{-2}, \delta = 10^{-1}, \mathrm{Br} = 10^{-1}$ and $Q = 0.1$ were used. We observe that near the start of the exchanger, where z is small, the recirculation regions II and III are relatively unaffected by the heat-exchange boundary at $y = 0$ (they appear as light-coloured regions). Once the boundary layer has diffused into region II, the heat-exchange process is aided by the recirculating flow, and so the width of region I, or the amount of inter-cavity flow, critically affects the thermal mixing properties of an SSHE. As far as channelling is concerned, the light areas of Fig. 8 may be considered "bad" and the dark areas "good". As expected, for a given z the maximum temperature in Fig. 8 invariably occurs at the boundary between regions II and III; a qualitative glance at the figure reveals however that, since at $z = 1$ no light-coloured regions remain, channelling is not present in this example.

A comparison of the temperature profiles predicted by the averaged model (22)–(27) and the 3D numerical "modelling" results of Sect. 3.3 is shown in Fig. 9 for two values of the transverse flux, namely $Q = 0$ and $Q = 0.1$. For comparison purposes, the 3D "modelling" results have been presented for a given $z = 0.4$ in the form of an average temperature in x (T_{AV}), and a temperature at a position adjacent to each blade at $x = 0.04$ and $x = 0.96$. From these results we can see that the temperature T_0 predicted by the averaged
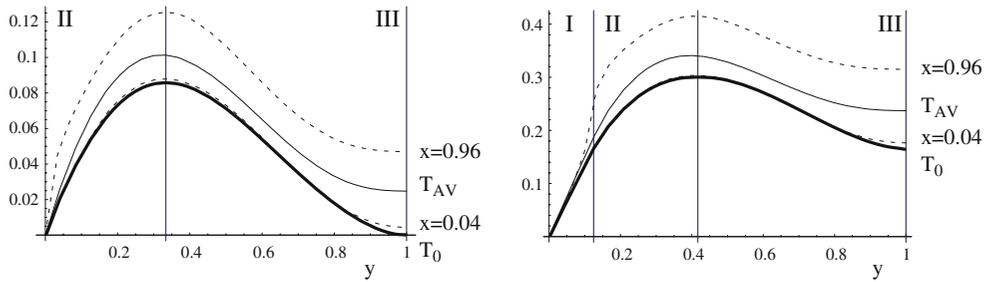
Fig. 9 A comparison between the averaged model of Sect. 4.1, (thick line), and the 3D "modelling" results of Sect. 3.3 at $z = 0.4$. The "modelling" results are given as the average $T_{AV} = \int_0^1 T dx$, (solid line), and at two positions $x = 0.04$ and $x = 0.96$, (dashed lines). The parameters used were $\gamma = 10^{-2}, \delta = 10^{-1}, \gamma \mathrm{Br} = 10^{-3}$. (a) Q = 0 and (b) Q = 0.1

model is usually less than T_{AV} but is very close to the temperature at one of the blades ($x = 0.96$). The fact that in general $T_0 < T_{AV}$ is entirely predictable, for the heat flux produced in the averaged model has been overestimated by the averaging. This fact is best illustrated by examining the results when $Q = 0$. In this case, the boundary condition for the region II/III problem is (24), so that the heat flow in this case is dominated by the heat flow into the stator rather than the slower flow near the insulated rotor. Evidently, including further terms from the asymptotic series would account better for the insulating boundary layer on the rotor.

4.3 Parametric study

We now investigate how the various problem parameters Q, Br, δ and γ affect the exchanger behaviour; one could consider a number of different metrics for heat transfer within the system such as flux averaged temperature or Nusselt numbers. Here we have chosen to use the maximum temperature of the output flow at $z = 1$ as our metric. This metric has the property that if ever channelling is indicated, $T_{\max}(\delta, \gamma, \mathrm{Br}, Q) \sim \geq 1$ (recall that under some circumstances dissipative viscous heating can make it possible for the output temperature to exceed the inlet temperature).

To illustrate the range of behaviours that can occur, Fig. 10 shows two-dimensional cross-sections in the four-dimensional parameter space. These cross-sections have been chosen so that they show extremes of behaviour encompassing regimes where no channelling at all takes place, and regimes where severe channelling is present. Once again, light-coloured regions show channelling and white regions indicate an output temperature greater than unity: in effect, a "cooler" that in fact heats.

In the first three examples ((a)–(c)) Q is fixed at zero and δ, γ and Br are varied. In plot 10(a) the maximum temperature at the exchanger outlet is plotted as a function of the diffusive properties of the material γ and the ratio of axial and transverse velocities δ. The model predicts a greater possibility of channelling when the axial velocities increase (decreasing residence times) and when thermal conductivity decreases. In Fig. 10(b), where δ is fixed and γ and Br vary, the isotherms are closer together near to the channelling regime where the output temperature exceeds unity; here relatively small decreases in γ produce more dramatic differences in the output temperature. The results shown in Fig. 10(c) where $Q = 0$ and γ is fixed show that increasing either δ or γBr (the axial through-flow or viscous dissipation respectively) results in larger output temperatures. Note that in each of the plots shown in Fig. 10((a)–(c)) the parameter variations lead to essentially monotonic variations in the output temperature.

The remaining three plots ((d)–(f)) in Fig. 10 illustrate the effects of varying Q, the inter-cavity through-flow while other parameters remain constant. Plots 10 (d), (e) suggest that, increasing the inter-cavity through-flow, will generally result in poorer heat transfer; when the size of region I increases, the thermal boundary layer takes longer to diffuse into the intra-cavity recirculating region, which mixes the heat more effectively. Essentially, it becomes harder for heat to exit from the fluid to the stator wall. However,
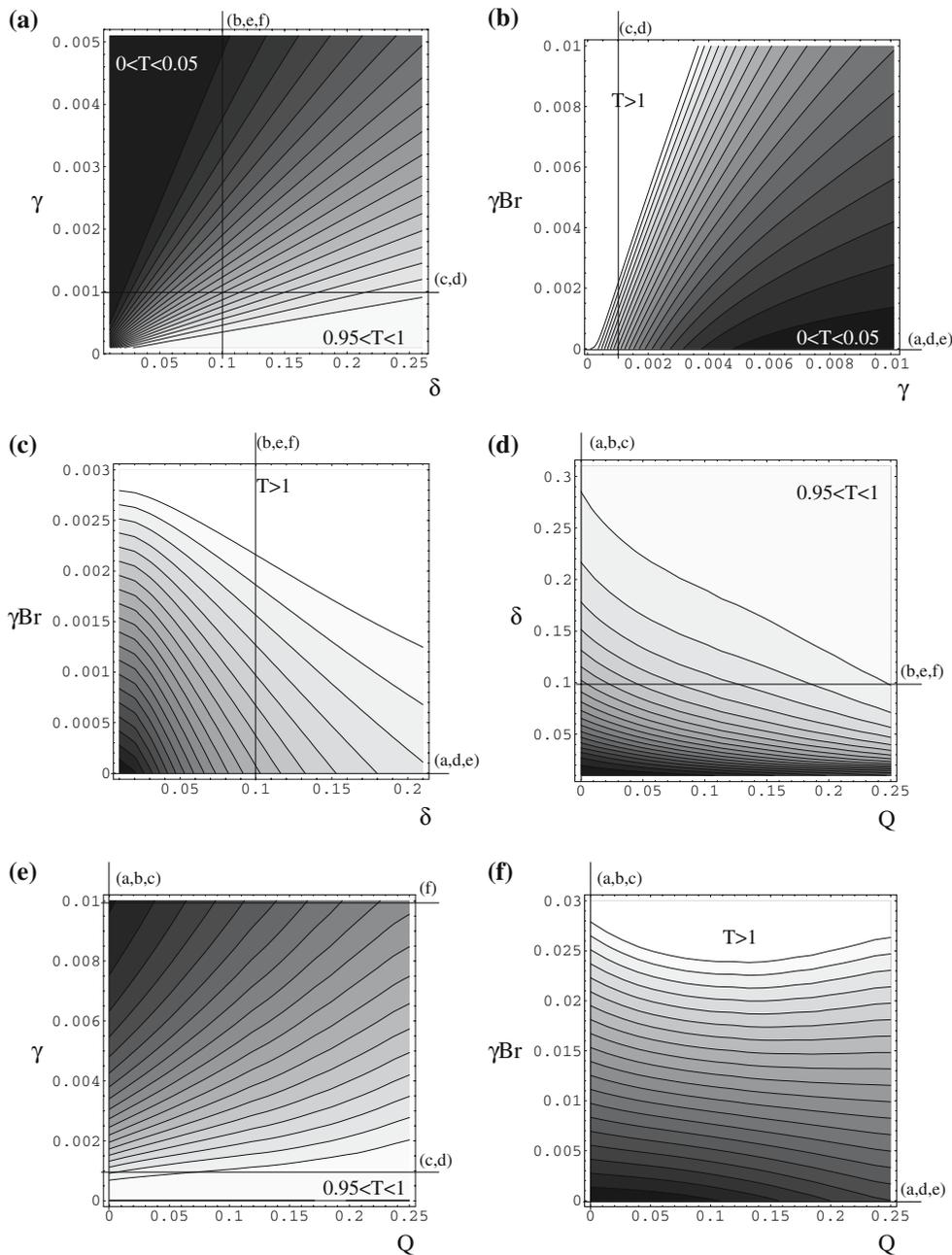
Fig. 10 Parametric plots of maximum temperature T_0 at the exchanger outlet $z = 1$ predicted by averaged model. The temperature contours are at intervals of 0.05 and the black regions are defined by $0 < T_0 < 0.05$. Dotted lines indicate projections of other graphs contained in this figure on the plane of each graph. (a) Q = 0, Br = 0, (b) Q = 0, $\delta = 10^{-1}$, (c) Q = 0, $\gamma = 10^{-3}$, (d) Br = 0, $\gamma = 10^{-3}$, (e) Br = 0, $\delta = 10^{-1}$ and (f) $\gamma = 10^{-2}$, $\delta = 10^{-1}$

once there is significant viscous dissipation within the exchanger, we observe in plot (f) that increasing Q can either increase or decrease the maximum temperature, which is a non-monotonic effect. Note that the viscous dissipation $(\mathrm{d}u/\mathrm{d}y)^2$ decreases monotonically as Q increases. The reduction in dissipation as a result of increasing the inter-cavity flux, competes with the associated poorer heat transfer due to the increase in size of region I, as seen in plots (d) and (e) of Fig. 10.

5 Summary and conclusions

The temperature evolution of a Newtonian fluid within an idealised SSHE has been studied in a physically realistic parameter regime. To our knowledge, this is the first theoretical (non-numerical) study to attempt to address the phenomenon of "channelling" in an SSHE that has included the effects of both three-dimensionality and heat transfer. The simultaneous inclusion of both multi-dimensional and thermal effects is complicated by the fact that the thermal problem necessarily involves advection, diffusion and dissipation. It is only through the use of asymptotic analysis and averaging methods that progress may be made.

A four-parameter model was studied which included material properties, geometrical variables of SSHEs and processing parameters. The analysis enables the key non-dimensional parameters that govern the industrial process to be identified and analysed. It it worth noting that the main assumptions of the study (namely laminar flow, large Péclet number, small aspect ratio and small reduced Reynolds number) hold for a very wide range of SSHEs. The analysis is therefore widely applicable to industrial processes involving SSHEs.

The solutions obtained compare well to a full numerical simulation, although the agreement is likely to improve markedly as the aspect ratio ϵ decreases. The asymptotic analysis that was used has the great advantage of leading to a numerical formulation that is markedly simpler than a full numerical simulation, and this allows the parametric dependence of the solutions to be investigated with ease. The asymptotics also allow the different flow topologies that result from different chamber leakage rates to be easily enumerated and explained.

A two-dimensional averaged model was then formulated and solved numerically, using "reconnection" boundary conditions that faithfully reflect the salient details of the flow inside an SSHE and its effect on the heat transfer that occurs. The averaged model allows easy identification of regimes where undesirable "channelling" may occur.

Finally, the methodology that has been developed allowed a parametric study to be performed. This focused on predicting the onset of "channelling". This allowed the identification of parameter regimes that resulted in dramatic changes in output temperature profiles. The effect of increasing blade through-flow and the associated dissipation, illustrated in Fig. 10, was also discussed.

In spite of the relative generality of the model presented, many further developments are possible. Key aims for the future include accounting for the dependence of viscosity on temperature and adding non-Newtonian effects (many foodstuffs processed in SSHEs are known to be pseudoplastic). It may also be possible to extend the analysis presented here to encompass multiphase materials (e.g. jams containing fruit segments or soups containing vegetable parts). Phase changes such as freezing may also take place in SSHEs (though these are usually considered to be undesirable) and it may be possible to use the methodology developed in this study to examine such scenarios.

It is also clear that, if more experimental data were to become available, comparison studies could be carried out to assess the accuracy of the results presented here. One reason why experimental data is inherently hard to gather is that, if any apparatus is added to the flow for the purpose of data collection, it is likely to be damaged by the scrapers.

References

1. Baccar M, Abid MS (1997) Numerical analysis of three-dimensional flow and thermal behaviour in a scraped surface heat exchanger. Rev Gen Therm **36**:782–790

2. Sun K-H, Pyle DL, Fitt AD, Please CP, Baines M, Hall-Taylor N (2004) Numerical study of 2D heat transfer in a scraped surface heat exchanger. Computers and Fluids **33**:869–880
3. Sun K-H, Pyle DL, Baines M, Hall Taylor N, Fitt AD (2006) Velocity profiles and frictional pressure drop for shear thinning materials in lid driven cavities with fully developed axial flow. Chem Eng Sci **61**:4697–4706
4. Duffy BR, Wilson SK, Lee MEM, (this issue) A model of fluid flow in a scraped-surface heat exchanger. J Eng Math
5. Fitt AD, Please CP (2001) Asymptotic analysis of the flow of shear-thinning foodstuffs in annular scraped heat exchangers. J Eng Math **39**:345–366
6. Wang W, Walton JH, McCarthy KL (2000) Mixing in scraped surface heat exchanger geometry using MRI. J Food Proc Eng **23**:403–418
7. Wang W, Walton JH, McCarthy KL (1999) Flow profiles of power law fluids in scraped surface heat exchanger geometry using MRI. J Food Proc Eng **22**:11–27
8. Pyle DL, Sun K-H, Hall-Taylor N, Fitt AD, Please CP, Baines M (2004) Numerical studies of heat transfer with shear thinning fluids in scraped surface heat exchangers. In: Proceedings of the 9th International Congress on Engineering and Food